CIRCUITS SYSTEMS SIGNAL PROCESSING
VOL. 25, NO. 2, 2006, PP. 201–224

DOI: 10.1007/s00034-005-2504-6

ON THE APPLICATIONS OF THE FREQUENCY-RESPONSE MASKING TECHNIQUE IN ARRAY BEAMFORMING*

Yongzhi Liu [1] *and Zhiping Lin*[1]

Abstract. The frequency-response masking (FRM) technique is well known to be very efficient in the implementation of finite impulse response (FIR) filters with sharp transition bands. As sensor array beamforming is closely related to FIR filtering, the feasibility of the applications of the FRM technique in array beamforming is investigated in detail in this paper. On one hand, it is shown that there is a limitation in applying the FRM technique in passive array beamforming. On the other hand, for active array beamforming, a novel combination of the concept of effective aperture and the FRM technique does lead to the synthesis of desirable beamformers. These beamformers have effective beampatterns with sharp transition bands and low sidelobes, and can be implemented with fewer sensors than other design techniques.
Key words: Frequency-response masking technique, array beamforming, effective aperture, FIR filters.

1. Introduction

The frequency-response masking (FRM) technique [11] is well known to be very efficient in the implementation of finite impulse response (FIR) filters with sharp transition bands. In contrast to high-order FIR filters designed using conventional methods such as windowing, least-squares, or minimax methods, FIR filters designed by the FRM technique consist of a group of less-complicated subfilters organized in a special structure. Compared to other direct FIR filter implementation methods, the implementation of FRM filters is less demanding computationally.

Digital array beamforming has been widely and successfully deployed in military and commercial applications [1], [4], [15]. By exploiting the spatial diversity of sensors, digital sensor array beamformers receive/transmit signals from/to specific directions and attenuate signals from/to other directions, even if both the desired signals and the interferences occupy the same temporal frequency

* Received February 2, 2005; revised September 16, 2005.
[1] School of Electrical and Electronic Engineering, Nanyang Technological University, Singapore 639798, E-mail for Lin: ezplin@ntu.edu.sg; E-mail for Liu: liuyongzhi@pmail.ntu.edu.sg

band. A conventional beamformer linearly combines the spatially sampled time sequences from each sensor to obtain a scalar output time sequence in the same manner in which an FIR filter linearly combines temporally sampled data. The correspondence between FIR filtering and beamforming is closest when the beamformer operates at a single temporal frequency and the array geometry is linear and equispaced [22], i.e., a uniform linear array (ULA) beamformer. For a ULA beamformer, its response can be directly mapped to the frequency response of a corresponding FIR filter. The analogy between FIR filters and ULA beamformers led to the applications of FIR filter design methods in array beamformer synthesis [21], [22].

Beampattern characteristics fundamentally affect how the acquired sensor data are processed. The most important parameters are mainlobe width, sidelobe level, and transition bandwidth. In general, sharp transition bands and low sidelobes are desirable properties of a beamformer as the transition bandwidth determines the spatial discrimination capability and the sidelobe level determines the interferences and noise suppression capability. Analogous to FIR filter design, the spatial discrimination capability of a ULA beamformer depends on the size of the spatial aperture. To achieve a desirable beampattern with sharp transition bands and low sidelobes, beamformers designed by conventional methods require a large number of sensors leading to high costs and heavy computational loads. Although FIR filter design methods, such as windowing methods, have been applied to array beamformer synthesis in the aspect of sidelobe level reduction [22], no attempt has been made to reduce the number of sensors while maintaining the same transition bandwidth and sidelobe level. This has motivated the present feasibility study on the applications of the FRM technique in array beamforming, with an emphasis on reducing the number of sensors and hence the computational complexity of the associated beamforming algorithm.

To facilitate the discussion on array beamforming using the FRM technique, some filter implementation issues such as the computational complexity, the required memory, and the effective filter length are studied in detail in Section 2. Passive array beamforming using the FRM technique is presented in Section 3, and an analysis is carried out to show the infeasibility of reducing the number of sensors. Subsequently, active array beamforming based on the concept of effective aperture [5] and the FRM technique is discussed in Section 4. Using the proposed method, it is possible to reduce the number of sensors for active array beamforming, as verified by simulations. Generalizations to two-dimensional (2D) active array beamforming are discussed in Section 5 and a conclusion is given in Section 6.

2. Frequency-response masking technique

The FRM technique [11] is an efficient method for implementing linear-phase FIR filters with sharp transition bands. This technique has become the method of choice primarily because of its considerable complexity reduction in implemen-

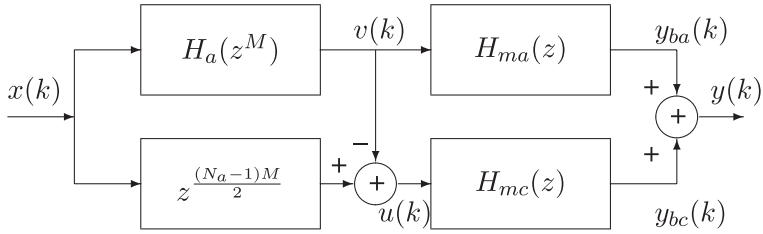

Figure 1. A realization structure for a filter using the FRM technique.

tation compared to other FIR filter design alternatives, such as those in [6], [7], [19]. Further complexity reduction has been an active topic of research recently [8]–[10] and is one of the objectives of this special issue. As the FRM technique is maturing, it is of particular interest to look for applications in other areas. To facilitate the discussion on the FRM applications in array beamforming in Section 3, implementation issues such as the computational complexity, the required memory, and the effective filter length are studied in this section. The study of these issues is of interest in itself as well.

A realization structure for a filter using the FRM technique is illustrated in Figure 1, in which several subfilters are involved. They are a bandedge shaping filter $\{h_a(n)\}$ and two masking filters $\{h_{ma}(n)\}$, $\{h_{mc}(n)\}$, whose transfer functions are given by

$$\begin{aligned} H_a(z) &= \sum_{n=0}^{N_a-1} h_a(n)z^{-n}, \\ H_{ma}(z) &= \sum_{n=0}^{N_{ma}-1} h_{ma}(n)z^{-n}, \\ H_{mc}(z) &= \sum_{n=0}^{N_{mc}-1} h_{mc}(n)z^{-n}. \end{aligned} \tag{1}$$

Let $\{h_{ua}(n)\}$ be the interpolated filter obtained from $\{h_a(n)\}$ with $M-1$ zeros inserted between adjacent taps. As $\{h_{ua}(n)\}$ is normally assumed to be an even-order linear phase filter, its complementary filter can be obtained easily with a simple delay line. The transition bandwidth of $\{h_{ua}(n)\}$ is $1/M$ of that of $\{h_a(n)\}$, and multiple spectrum replicas appear in $[0, 2\pi)$. Using properly designed masking filters, some unwanted spectrum replicas are removed while the rest are integrated in passband synthesis. Denote N_m the maximum length of the masking filters, i.e., $N_m = \max(N_{ma}, N_{mc})$, and adjust the length of both masking filters to N_m by appropriately zero-padding if necessary.

Although FRM filtering is well known to be computationally efficient, it was found that its implementation requires well-organized memory to hold a large number of input samples [14], where the discussion was focused on field pro-

grammable gate array implementation of digital filters synthesized using the FRM technique. Referring to Figure 1, assume that the input samples are divided into M subgroups of N_a samples each. When a new sample $x(k)$ is available, one subgroup is updated by replacing the oldest sample with $x(k)$. The subgroup is filtered by $\{h_a(n)\}$ as

$$v(k) = \sum_{n=0}^{N_a-1} h_a(n)x(k - nM), \tag{2}$$

which requires N_a multiplications (for direct form implementation). The intermediate output is subsequently filtered by the masking filters, leading to

$$y_{ba}(k) = \sum_{n=0}^{N_m-1} h_{ma}(n)v(k - n), \tag{3a}$$

$$y_{bc}(k) = \sum_{n=0}^{N_m-1} h_{mc}(n)u(k - n), \tag{3b}$$

where $u(k) = x\left(k - \frac{(N_a-1)M}{2}\right) - v(k)$ and about $2N_m$ multiplications are required (or to be exact, $N_{ma} + N_{mc}$). Because $y_{ba}(k)$ and $y_{bc}(k)$ are functions of $N_m - 1$ previous outputs of $\{h_{ua}(n)\}$, the final output, $y(k) = y_{ba}(k) + y_{bc}(k)$, is actually a linear combination of the following input samples:

$$x(k - (N_aM + N_m - M - 1)), \qquad x(k - (N_aM + N_m - M - 2)), \ldots, x(k), \tag{4}$$

where $x(n) = 0$ for $n < 0$. As we can see, the computational complexity is $N_a + 2N_m$ multiplications per sample when k is larger than $N_aM + N_m - M$. Meanwhile, memory holding N_aM latest input samples and $2N_m$ intermediate outputs is constantly maintained throughout the filtering process.

Assume that the condition $N_m \geq M$ holds ($N_m < M$ is not of interest practically, as will be discussed shortly); then the effective filter length of the preceding FRM filter is equal to $N_aM + N_m - M$ [11]. Let F_s be the sampling frequency and ΔF be the transition bandwidth of a designed lowpass FRM filter. The normalized transition bandwidth of the filter is defined as $\Delta f = \Delta F/F_s$. The FRM technique is efficient when Δf is very small, i.e., $\Delta f \ll 1/16$, which is assumed throughout the paper (note that Δf is the same as β introduced in [12]). To meet the same specifications, the length of an optimum (Remez) FIR filter, N_o, is slightly shorter than the effective filter length of the FRM filter [12].

Some key features related to filter implementation between the FRM filter and the corresponding optimum FIR filter are compared in Table 1; these are the effective filter length, the memory size, and the computational complexity (in terms of number of multiplications). Despite the slightly longer effective filter length and the increased memory size for the case of $N_m \geq M$, the computational complexity of the FRM filter is considerably reduced compared to the optimum filter. The

Table 1. Comparison of FRM filters and optimum filters

	Effective filter length	Memory size	Computational complexity	Condition
FRM filters	$N_aM + N_m - M$	$N_aM + 2N_m$	$N_a + 2N_m$	$N_m \geq M$
Optimum filters	N_o	N_o	N_o	

reduction in computational complexity is mainly attributed to the sparseness of the interpolated filter $\{h_{ua}(n)\}$.

In the FRM filter design, the factor M affects the complexity of the subfilters. As will be seen in Section 3, the effective filter length of the FRM filter is actually the total number of sensors to be deployed in passive array beamformers. It is therefore important to establish the relationship between M and N_m.

For a given M, the transition bandwidths of the masking filters are

$$\Delta_{ma} = \frac{2\pi - w_{ap} - w_{as}}{M}, \tag{5a}$$

$$\Delta_{mc} = \frac{w_{ap} + w_{as}}{M}, \tag{5b}$$

where w_{ap} and w_{as} represent the passband and stopband cutoff frequencies of the bandedge shaping filter, respectively [11]. Define the mean of Δ_{ma} and Δ_{mc},

$$\Delta_{mid} = (\Delta_{ma} + \Delta_{mc})/2 = \pi/M, \tag{6}$$

which is a function of M.

Given a Δf and magnitudes of the passband and stopband ripples δ_1 and δ_2, the filter length can be approximated by the well-known Kaiser's equation [20],

$$N = \frac{-20\log_{10}\sqrt{\delta_1\delta_2} - 13}{14.6\Delta f} + 1. \tag{7}$$

For the same magnitudes of the ripples, the filter lengths N_{ma}, N_{mc}, and N_{mid}, corresponding to the transition bandwidth Δ_{ma}, Δ_{mc}, and Δ_{mid}, respectively, satisfy the following inequality:

$$N_m = \max(N_{ma}, N_{mc}) \geq N_{mid} \geq \min(N_{ma}, N_{mc}). \tag{8}$$

It is assumed that the ripple magnitudes of the masking filters, δ_1 and δ_2, are 15% smaller than the allowed magnitudes of the designed filter, δ_p and δ_s [11]. Using (6) and (7), it can be found that $N_{mid} \geq M$ is equivalent to

$$\delta_1\,\delta_2 = 0.85^2\delta_p\delta_s \leq 10^{0.73/M-2.03}. \tag{9}$$

It follows from (8) that $N_m \geq M$ when (9) is satisfied. As M is a positive integer,

$$\delta_p\,\delta_s < 1.384 \times 10^{-2.03} \tag{10}$$

gives a sufficient condition for $N_m \geq M$ in terms of ripple magnitudes of the

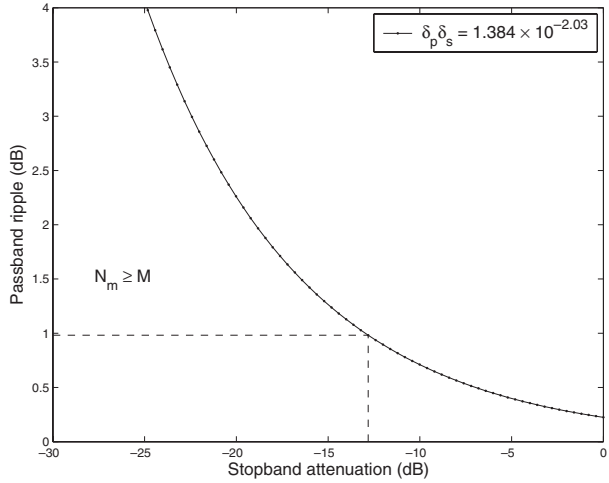

Figure 2. Condition for $N_m \geq M$. Maximum passband ripple δ_p and minimum stopband attenuation δ_s are expressed in decibels.

designed filter, as depicted in Figure 2. It is obvious from this figure that for nontrivial FIR filters designed by the FRM technique, i.e., filters with maximum passband ripple less than 1 dB and minimum stopband attenuations larger than 13 dB, $N_m \geq M$ is always satisfied. For example, in the design example given in [11], the allowed maximum passband ripple $\delta_p = 0.0115$ (0.2 dB) and minimum stopband ripple $\delta_s = 0.01$ (40 dB) fall inside the region of $N_m \geq M$ indicated in Figure 2. Hence, we should have $N_m \geq M$. Indeed, it was shown in an example of [11] that for each M ($M = 2, \ldots, 14$), the corresponding N_m that resulted in minimum filter complexity was always greater than M. For example, for $M = 6$ or 9, we have $N_m = 33$ or 41. Thus, we conclude that it is generally true that N_m is no less than M. This result has an important implication in the next section.

3. Passive array beamforming using the FRM technique

In this section we begin with a review on the relationship between narrowband array beamforming and FIR filtering [22], and then discuss the feasibility of the applications of the FRM technique in passive array beamforming.

3.1. Passive array beamforming

The frequency response of an FIR filter with an impulse response $\{h(n)\}$, $0 \leq n \leq N-1$, is given by

$$H(\omega) = \sum_{n=0}^{N-1} h(n)e^{-j\omega n}, \tag{11}$$

which represents the response of the filter to a complex sinusoid of frequency ω. Similarly, the beamformer response is defined as the amplitude and phase presented to a complex plane wave, $e^{j\omega k}$, as a function of direction of arrival (DOA) θ and frequency ω. For an N-sensor beamformer with an aperture function that is the same as the FIR filter $\{h(n)\}$, the beamformer response is [22]

$$H(\theta, \omega) = \sum_{n=0}^{N-1} h(n) e^{-j\omega\tau_n(\theta)}, \tag{12}$$

where $\tau_0(\theta) = 0$ and $\tau_n(\theta)$, $1 \leq n \leq N-1$, represents the time delay due to propagation relative to the first sensor element.

The correspondence between FIR filtering and beamforming is closest when the beamformer operates at a single temporal frequency $\omega = \omega_o$ and the array geometry is linear and equispaced, i.e., a ULA beamformer. Let the intersensor spacing be d, the wavelength be λ, and the DOA relative to broadside be θ. Then the delay can be expressed as $\tau_n(\theta) = 2\pi n \frac{d \sin\theta}{\lambda\omega_o}$ and the relationship between the temporal frequency ω in FIR filtering and the direction θ in array beamforming can be identified as $\omega = 2\pi \frac{d \sin\theta}{\lambda}$. Thus, the temporal frequency in FIR filtering corresponds to the sine of direction in narrowband ULA beamforming. To avoid spatial ambiguity and increase the spatial resolution of a ULA beamformer, $d = \lambda/2$ is usually used and, in such a case, each $\theta \in [-\pi/2, \pi/2)$ is uniquely mapped to one $\omega \in [-\pi, \pi)$. The corresponding beamformer response becomes $H(\theta, \omega_o) = H(\pi \sin\theta) = H(\phi)$.

The analogy between FIR filtering and ULA beamforming led to the applications of FIR filter design methods in array beamformer synthesis [21]. As the FRM technique is successful in FIR filter synthesis with considerable reduction in computational complexity, it is natural to ask whether we could apply the FRM subfilters as aperture functions to ULAs to achieve desirable beampatterns with fewer sensors compared with traditional beamformer design methods. The answer is negative for passive arrays, as will be discussed briefly in the following section. To simplify the presentation, $H(\phi)$ is adopted as the response of the beamformer with an aperture function $\{h(n)\}$.

3.2. Interleaved linear array beamformers

An intuitive idea in applying the FRM technique to array beamforming with the aim of reducing the number of sensors is to construct a linear sensor array consisting of several subarrays, each associated with one FRM subfilter. A linear array comprising one N_m-sensor dense ULA with intersensor spacing $d = \lambda/2$ and one N_a-sensor sparse ULA with intersensor spacing $Md = M\lambda/2$ is shown in Figure 3. This beamformer is called an interleaved linear array beamformer. Four subbeamformers are formed when the subfilters $\{h_{ma}(n)\}$ and $\{h_{mc}(n)\}$ are applied as aperture functions for the dense ULA and $\{h_a(n)\}$ and its complementary filter, $\{h_c(n)\}$, are applied for the sparse ULA. Without loss of generality, let

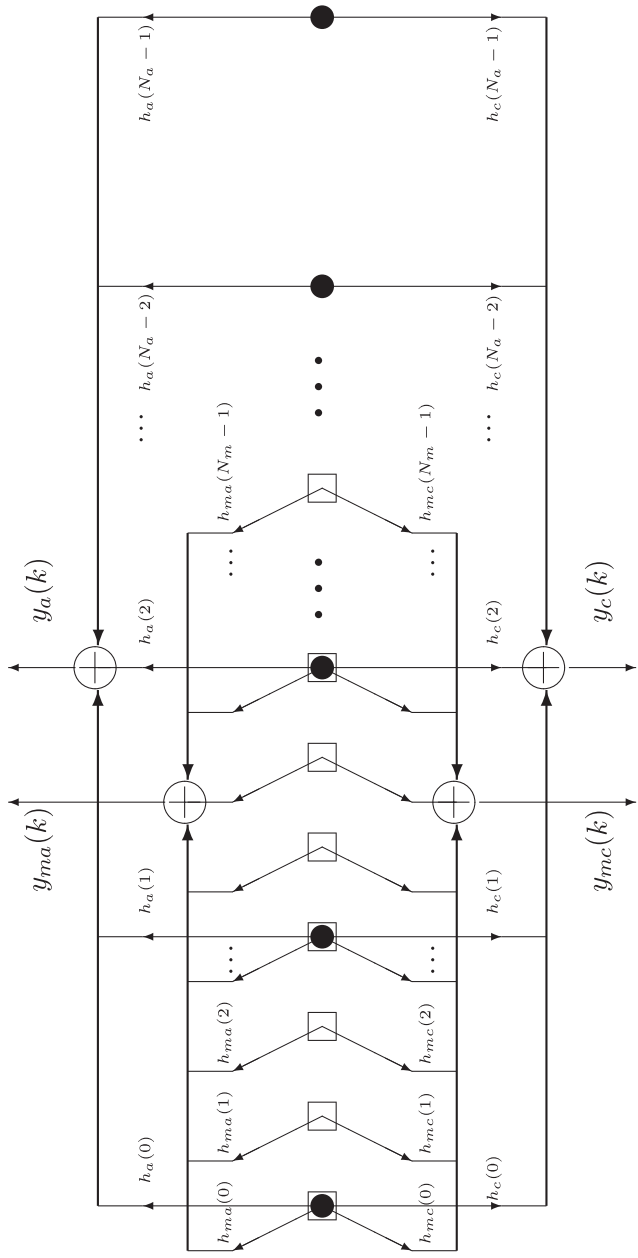

Figure 3. An interleaved linear array beamformer using one sparse ULA in solid circles and one dense ULA in squares with $M = 3$.

the phase be zero at the first sensor, i.e., $x_0(k) = e^{j\omega_o k}$. The four subbeamformer outputs responding to the signal from θ can be written as

$$y_a(k) = x_0(k) \sum_{n=0}^{N_a-1} h_a(n)e^{-jnM\phi} = e^{j\omega_o k} H_a(M\phi),$$

$$y_c(k) = x_0(k) \sum_{n=0}^{N_a-1} h_c(n)e^{-jnM\phi} = e^{j\omega_o k} H_c(M\phi),$$

$$y_{ma}(k) = x_0(k) \sum_{n=0}^{N_m-1} h_{ma}(n)e^{-jn\phi} = e^{j\omega_o k} H_{ma}(\phi),$$

$$y_{mc}(k) = x_0(k) \sum_{n=0}^{N_m-1} h_{mc}(n)e^{-jn\phi} = e^{j\omega_o k} H_{mc}(\phi).$$

However, if we linearly combine these subbeamformer outputs, for example, by simply adding them together, we are unable to generate the desirable output in the form of $e^{j\omega_o k}(H_a(M\phi)H_{ma}(\phi) + H_c(M\phi)H_{mc}(\phi))$. Despite the similarity of the interleaved linear array beamformer to a temporal FRM filter, we fail to obtain the required array response $H(\phi) = H_a(M\phi)H_{ma}(\phi) + H_c(M\phi)H_{mc}(\phi)$. The reason lies in the difference between temporal filtering and array beamforming. As analyzed in Section 2, in the FRM filtering process, although $N_a + 2N_m$ multiplications are required for each instance, N_a input samples from the memory are involved for $H_a(z^M)$ and $2N_m$ intermediate outputs from the memory for $\{v(n)\}$ and $\{u(n)\}$. Because these intermediate outputs in turn are linear combinations of past input samples, the FRM filter output at each instance is in fact a linear combination of past samples given in (4), most of which are available in the memory. Throughout the whole filtering process, memory for holding the signal samples is indispensable. However, in array beamforming, the spatial samples are linearly combined at each snapshot. There exists no mechanism to hold the spatial samples similar to that in the temporal filtering process. With the limited number of spatial samples provided by the proposed sensor array in Fig. 3, beamforming equivalent to that with a ULA with N_o sensors cannot be achieved.

3.3. Multiple subarray beamformers

Having shown the infeasibility of applying the FRM technique in the interleaved linear array beamformers, we consider another kind of beamforming, which is closely analogous to the FRM technique.

Figure 4 depicts a multiple subarray beamformer. It consists of N_a subarrays, each of which consists of N_m sensors with intersensor spacing $d = \lambda/2$. Adjacent subarrays are displaced by $Md = M\lambda/2$. In addition, sensors at the common nodes are shared by neighboring subarrays. The spatial samples in each subarray

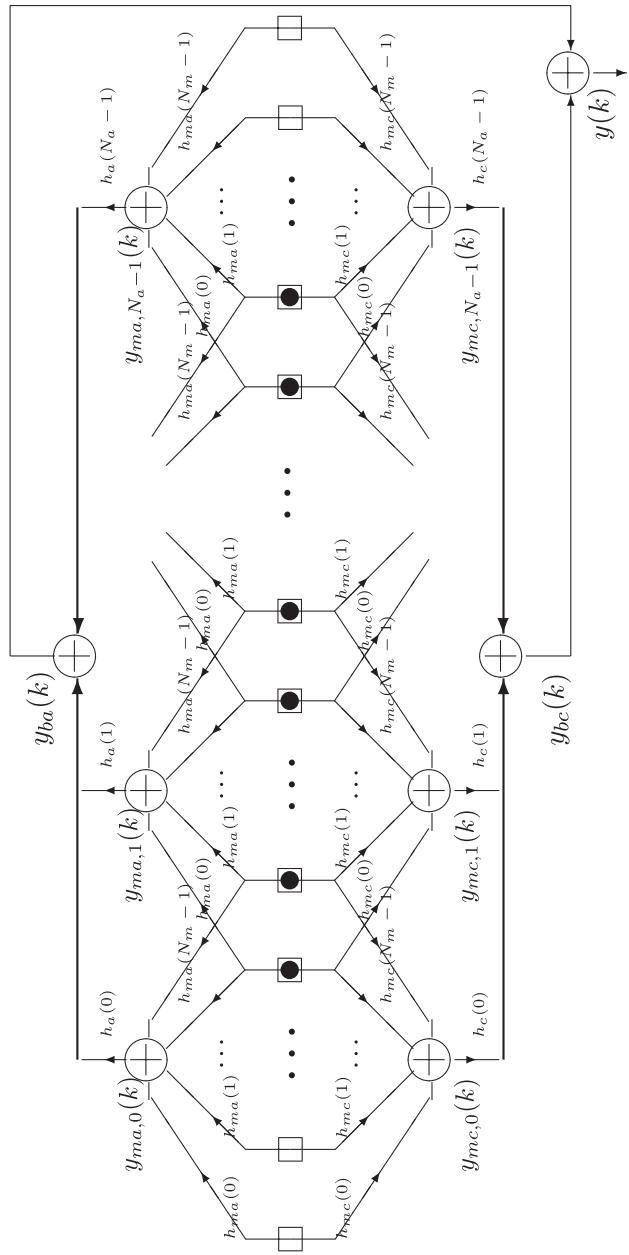

Figure 4. A typical multiple subarray beamformer with $N_m = M + 2$. The sensors shared by neighboring subarrays are marked with a dot in a square.

are shared and weighted with the aperture functions $\{h_{ma}(n)\}$ and $\{h_{mc}(n)\}$ simultaneously. Subsequently, the subarray outputs are weighted with aperture functions $\{h_a(n)\}$ and $\{h_c(n)\}$. Assume that a narrowband plane wave impinges upon the linear array from angle θ relative to broadside, and the spatial sample at the first sensor is $x_0(k) = e^{j\omega_o k}$. It can be easily shown that the beamformer output $y(k)$ is

$$y(k) = y_{ba}(k) + y_{bc}(k) = e^{j\omega_o k}\left(H_a(M\phi)H_{ma}(\phi) + H_c(M\phi)H_{mc}(\phi)\right) \quad (13)$$

and the beamformer response is

$$H(\phi) = H_a(M\phi)H_{ma}(\phi) + H_c(M\phi)H_{mc}(\phi), \quad (14)$$

which is identical to an FRM filter response.

From the array layout of the above multiple subarray beamformer, it is clear that, with the assumption of $N_m \geq M$, the total number of sensors is equal to $N_a M + N_m - M$, which is slightly larger than N_o, the number of sensors for an equivalent ULA beamformer whose aperture function is designed using the Remez algorithm. For completeness, we mention that for the case of $N_m < M$, the total number of sensors, $N_a N_m$, could be smaller than N_o. However, as we discussed in the previous section, the resultant FRM filter would be a poor one unable to meet the required frequency specifications. Again, we fail to reduce the number of sensors by applying the FRM to multiple subarray beamformers.

In summary, we have shown the infeasibility of applying the FRM technique in passive array beamforming through an analysis of the difference between temporal filtering and passive array beamforming. Nevertheless, for active array beamforming, we will show in the next section that the FRM technique can be applied to synthesize active array beamformers with a reduced number of sensors.

4. Active array beamforming using the FRM technique

Active array beamforming is widely deployed in contemporary radar and sonar systems, ultrasonic diagnostic systems, etc., to remotely measure environment parameters or detect objects of interest. An active array beamformer comprises a multitude of sensor elements. Subsets of these elements form the apertures that are used for transmission or reception. At each excitation, the transmitted waves are weighted before propagating. The wavefront is then reflected when it hits the object. The scattered wavefront is resampled and converted to electric signals by the receiving elements.

As the number of sensors directly affects the system cost, Von Ramm et al. were among the first to propose an approach to reduce the number of elements in a linear array while minimizing grating lobes caused by sparseness of the array layout [23]. They proposed different spacings for the transmitting and receiving elements so that the transmitting and receiving grating lobes could be moved

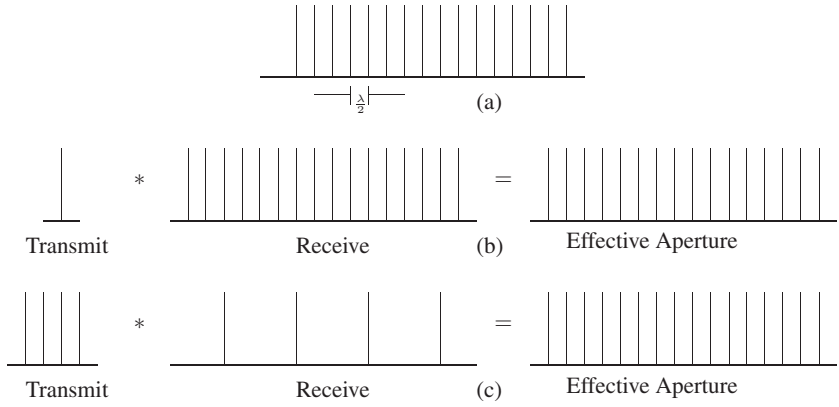

Figure 5. (a) Example of a "desired effective aperture" with element spacing $\lambda/2$. (b,c) Two different combinations of transmitting and receiving aperture functions that yield the same desired effective aperture in (a).

to different positions in the two-way radiation pattern where their contributions would destructively interfere. The basic idea behind this approach is the concept of effective aperture of an active array, which will be briefly reviewed here.

Let $\{h_t(n)\}$ and $\{h_r(n)\}$ denote the aperture functions associated with the transmitting and receiving arrays, respectively. The effective aperture of an active array is the receiving aperture which would produce an identical two-way radiation pattern if the transmitting aperture were a point source [5]. Mathematically, the effective aperture function is simply the convolution of $\{h_t(n)\}$ and $\{h_r(n)\}$, i.e.,

$$h_e(n) = h_r(n) * h_t(n), \tag{15}$$

where $*$ represents the convolution operation. Hence, unlike for the passive array, one can come up with the same effective aperture function with different combinations of $\{h_t(n)\}$ and $\{h_r(n)\}$. This was investigated in detail in the context of designing sparse linear arrays suitable for imaging systems [3], [16], [17].

We now briefly review a design method for sparse linear arrays [16]. Figure 5 shows an example of an effective aperture. In this example, the effective aperture is rectangular, with 16 elements and $\lambda/2$ element spacing. There are many different ways of selecting sparse transmitting and receiving aperture functions to yield the same effective aperture and the corresponding two-way radiation pattern. For example, we can use a single-element transmitting array and a 16-element receiving array with $\lambda/2$ spacing, as shown in Figure 5b. Alternatively, we can use a four-element transmitting array with $\lambda/2$ spacing and a four-element receiving array with 2λ spacing, as in Figure 5c. As can be seen, the latter design uses only 8 elements instead of the 16 elements of the former. In this example, the aperture functions for the transmitting and receiving arrays are rectangular. In

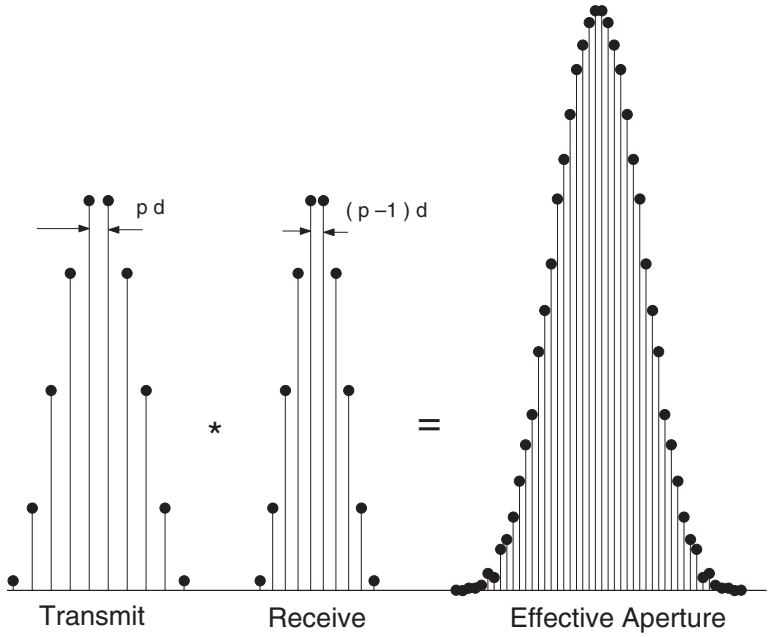

Figure 6. Aperture functions and effective aperture of a VSA with $p = 3$ and $\cos^2(\cdot)$ apodized functions.

practice, apodization can be used to control the shape of the effective aperture, offering more flexibility in designing an active array [16].

Among the various strategies for designing sparse arrays proposed in [16], the best one is the vernier sparse array (VSA), which is analogous to a linear vernier scale. In a VSA, by spacing the transmitting elements pd apart and the receiving elements $(p-1)d$ apart, where p is an integer, the convolution of the aperture functions will yield an effective aperture with elements spaced d apart. Figure 6 shows the aperture functions and the associated effective aperture of a VSA consisting of a 10-element transmitting array and a 10-element receiving array.

Note that all the existing methods for designing an active array using the concept of effective aperture [2], [3], [16], [17] tried to either avoid the grating lobes by eliminating the periodicity of the sparse arrays or attenuate the grating lobes by introducing nulls in the effective aperture functions. Using the FRM technique, it will be shown next that instead of suppressing all the grating lobes completely, some of them can be integrated in mainlobe synthesis by exploiting the complementary property of $\{h_a(n)\}$ and $\{h_c(n)\}$ and by properly designing the masking filters.

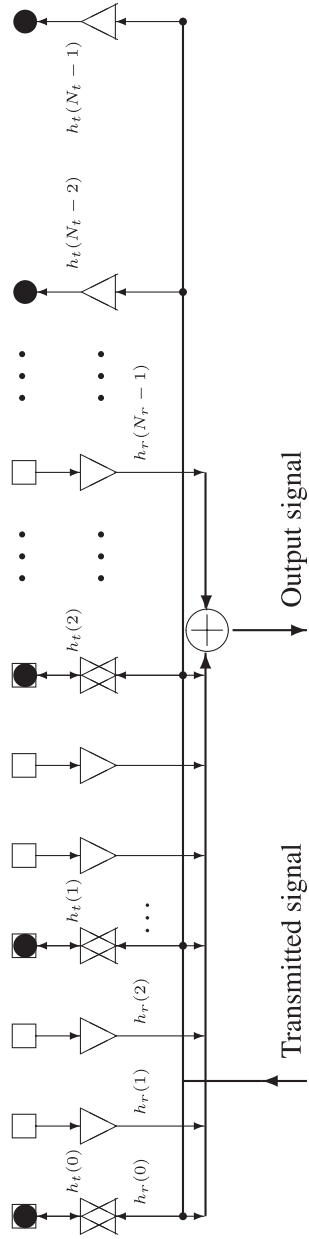

Figure 7. An AILA beamformer using a sparse transmitting ULA (in solid circles) and a dense receiving ULA (in hollow squares).

4.1. *Active interleaved linear array beamformers and effective aperture*

Motivated by our discussion on passive array beamforming, we propose an active interleaved linear array (AILA) beamformer comprising one transmitting array and one receiving array, as presented in Figure 7. The receiving array is an N_r-sensor ULA with intersensor spacing $d = \lambda/2$ and the transmitting array is an N_t-sensor uniform sparse array with intersensor spacing $Md = M\lambda/2$. As before, denote $\{h_t(n)\}$ and $\{h_r(n)\}$ the aperture functions associated with the transmitting and receiving arrays, respectively.

Take the first sensor on the left of the AILA as a reference and assume an object is located at θ relative to broadside in the far field. The narrowband signal (of center frequency ω_o) is weighted before transmitting. Without loss of generality, assume that the signal from the first sensor arrives at the object at phase 0. The resultant signal scattered from the object can be expressed as a summation of the signals from all transmitting elements,

$$x_s(k) = \sum_{n=0}^{N_t-1} h_t(n) e^{j\omega_o k} e^{-jnM\phi} = e^{j\omega_o k} H_t(M\phi). \tag{16}$$

The scattered plane wave is then spatially sampled by the receiving array and weighted with the receiving aperture function $\{h_r(n)\}$. The output signal becomes

$$y(k) = \sum_{n=0}^{N_r-1} h_r(n) x_s(k) e^{-jn\phi} = e^{j\omega_o k} H_t(M\phi) H_r(\phi). \tag{17}$$

By (15), the effective aperture of the AILA is

$$h_e(n) = h_r(n) * h_{ut}(n), \tag{18}$$

where

$$h_{ut}(m) = \begin{cases} h_t(m/M), & \text{for } m = 0, M, \ldots, (N_t - 1)M, \\ 0, & \text{otherwise.} \end{cases}$$

4.2. *Aperture functions by the FRM technique*

If $\{h_a(n)\}$ and $\{h_{ma}(n)\}$ are taken as the transmitting and receiving aperture functions, respectively, the output signal (17) becomes

$$y_{ba}(k) = e^{j\omega_o k} H_a(M\phi) H_{ma}(\phi). \tag{19}$$

When this process is repeated for the second excitation with the same transmitting signal, and the new transmitting and receiving aperture functions are $\{h_c(n)\}$ and $\{h_{mc}(n)\}$, respectively, the corresponding output signal becomes

$$y_{bc}(k) = e^{j\omega_o k} H_c(M\phi) H_{mc}(\phi). \tag{20}$$

Table 2. Frequency specifications of the FRM subfilters with $M = 8$

Subfilter	Filter length	Passband cutoff	Stopband cutoff
$\{h_a(n)\}$	35	0.472π	0.608π
$\{h_{ma}(n)\}$	39	0.076π	0.191π
$\{h_{mc}(n)\}$	31	0.174π	0.309π

The AILA beamformer output is the sum of the output signals (19) and (20) for the two excitations,

$$y(k) = e^{j\omega_o k}(H_a(M\phi)H_{ma}(\phi) + H_c(M\phi)H_{mc}(\phi)). \tag{21}$$

As seen from (19) and (20), the AILA beamformer actually makes use of two effective aperture functions

$$h_{ea}(n) = h_{ua}(n) * h_{ma}(n),$$
$$h_{ec}(n) = h_{uc}(n) * h_{mc}(n),$$

in which $\{h_{ua}(n)\}$ and $\{h_{uc}(n)\}$ are the interpolated filters of $\{h_a(n)\}$ and $\{h_c(n)\}$, respectively.

The novel combination of the concept of effective aperture and the FRM technique leads to the synthesis of desirable beamformers. Specifically, with a properly designed complementary filter pair and the masking filters, some of the grating lobes are integrated into the mainlobe synthesis instead of being suppressed completely. As a result, these beamformers have effective beampatterns with sharp transition bands and low sidelobes, and can be implemented with only $N_a + N_m$ sensors, much less than the $N_aM + N_m - M$ (or N_o) sensors required using conventional beamformer design techniques.

4.3. Computer simulations

A lowpass filter with a sharp transition band at $(0.174\pi, 0.191\pi)$ (corresponding to $(10°, 11°)$ in the azimuth domain) and minimum 40 dB stopband attenuation is synthesized. The frequency specifications of the FRM subfilters are presented in Table 2.

The subfilters are applied as the aperture functions of the AILA beamformer, and the simulation results are plotted in Figure 8. Assume that a sinusoidal signal with a frequency of 1 Hz is weighted with $\{h_a(n)\}$ and transmitted to the object. The transmitted waves reach the object at different phases. The scattered signal is resampled by the receiving array and weighted with the aperture function $\{h_{ma}(n)\}$. For the second excitation, the aperture function pair is changed to $\{h_c(n)\}$ and $\{h_{mc}(n)\}$. Two cases are simulated. *Case 1*: When a single object is located at 10° or 11°, the beamformer outputs of the object at 11° are severely

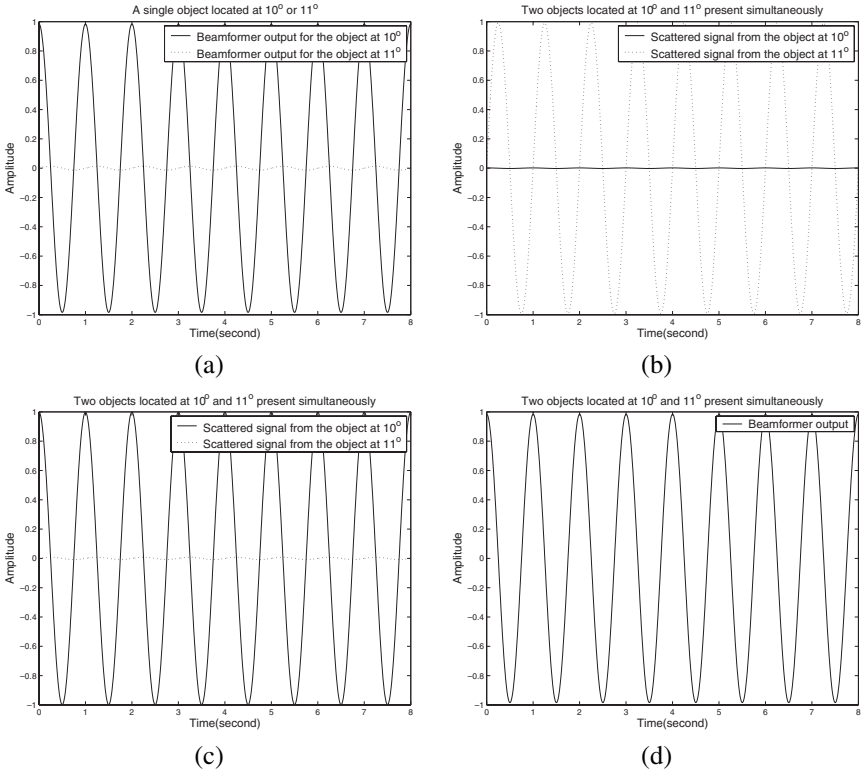

Figure 8. Spatial filtering simulation of the AILA beamformer. (a) The beamformer output signal when a single object is present at 10° or 11° relative to broadside. (b) Scattered signals from two objects present simultaneously at the first excitation. (c) Scattered signals from two objects present simultaneously at the second excitation. (d) The AILA beamformer output when two objects present simultaneously.

attenuated, as shown in Figure 8a. *Case 2*: When the two objects are present simultaneously, the scattered signals for the two excitations are shown in Figures 8b and 8c. Because of the difference in the distance, it is assumed, without loss of generality, that the scattered signal from the object at 11° experiences an extra $\pi/2$ phase difference. The scattered signals are then resampled and processed, leading to the AILA beamformer output in Figure 8d. By comparing Figure 8d with 8a, it can be seen that the signal from the object at 10° is dominant in the beamformer output.

We next generate the effective beampattern of the AILA beamformer. Assume that an object is located in the direction of θ in the far field. The beamformer output power is recorded when θ varies from 0° to 40° at an increment of 0.1°, as shown in Figure 9. The transition from 10° to 11° suggests the excellent spatial discrimination capability of this beamformer. With the aperture functions ob-

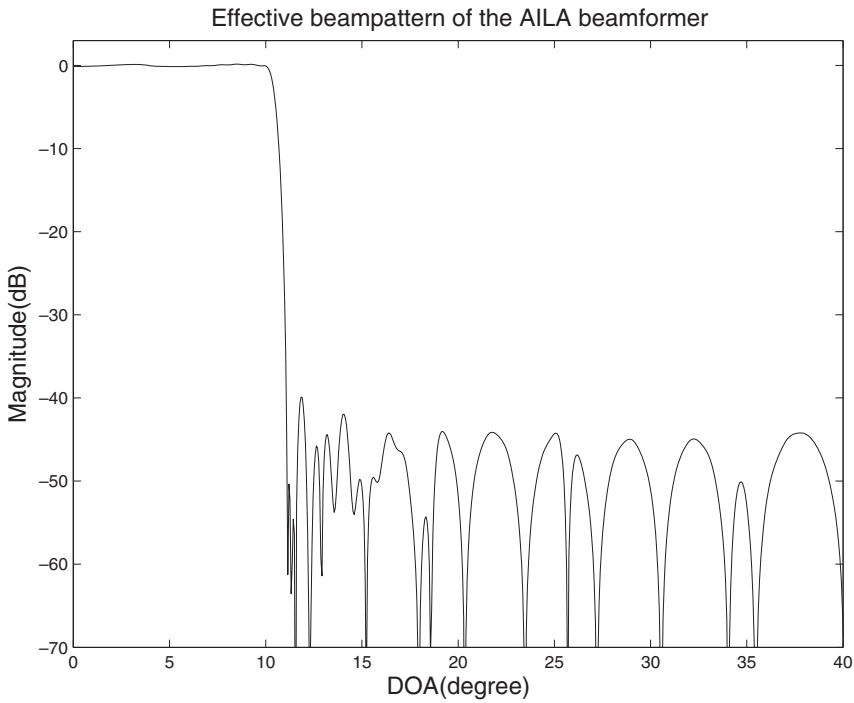

Figure 9. The effective beampattern of the AILA beamformer.

tained using the FRM technique, the AILA beamformer is capable of separating two closely spaced objects with only 74 sensors ($N_a = 35$, $N_m = 39$). However, to obtain a similar beampattern using a ULA beamformer whose aperture function is designed using the Remez algorithm, at least 215 sensors are required.

The only drawback of the AILA beamformer is that two excitations and two alternating aperture function pairs are required to complete one cycle. However, in narrow-beamwidth beamformer synthesis, only one excitation and one pair of aperture functions are needed. It can be regarded as a special case of the broad-beamwidth beamformer synthesis described above. In this case, the grating lobes caused by the sparseness of the transmitting array are attenuated by the properly designed receiving aperture function. For example, to obtain a desired beampattern with mainlobe cutoffs at ω_p and ω_s, the frequency specifications of the bandedge shaping filter and the masking filter are given in Table 3.

The synthesis of a narrow-beamwidth beamformer is compared for an AILA beamformer using the proposed method and a VSA beamformer using the method of [16]. Both the transmitting and receiving arrays of the VSA consist of 24 sensors, and $\cos^2(\cdot)$ is applied as the individual aperture function with $d = \lambda/2$

Table 3. Frequency specifications of the aperture functions in a narrow-beamwidth beamformer synthesis

Aperture functions	Type	Passband cutoff	Stopband cutoff
$\{h_a(n)\}$	Lowpass	$M\omega_p$	$M\omega_s$
$\{h_{ma}(n)\}$	Lowpass	ω_p	$(2\pi - M\omega_p)/M$

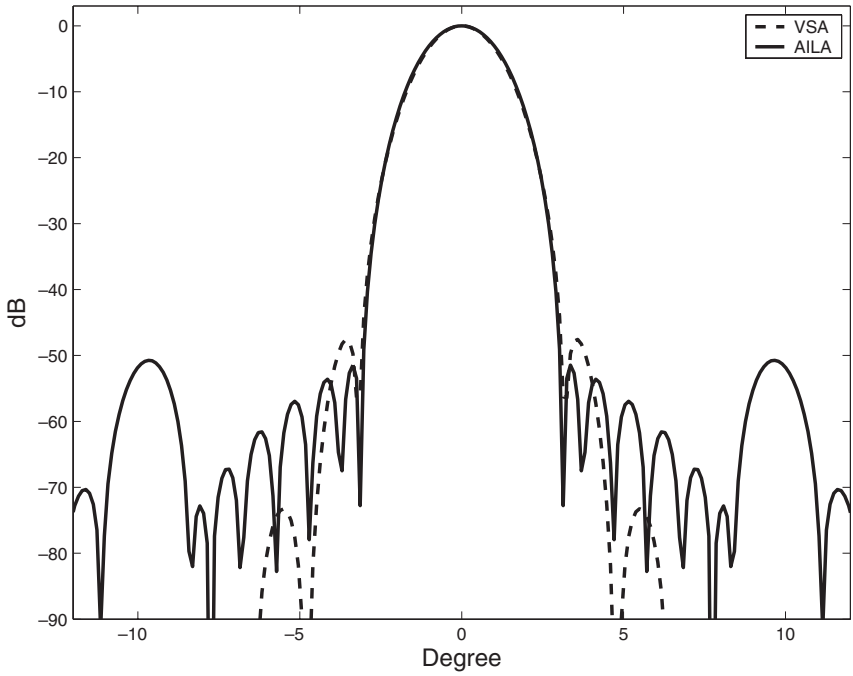

Figure 10. Beampattern comparison between the AILA beamformer ($N_t = 10$, $N_r = 30$, $M = 10$) and the VSA beamformer with $p = 3$ and $\cos^2(\cdot)$ aperture function (24 sensors in the transmitting array and 24 sensors in the receiving array).

and $p = 3$. Using the FRM technique, the transmitting and receiving aperture functions are redesigned for an AILA beamformer with a 10-sensor transmitting array and a 30-sensor receiving array. The effective beampatterns of the VSA and AILA beamformers are very similar in terms of transition bandwidth and sidelobe level, as shown in Figure 10. Note that the VSA beamformer needs 48 sensors, whereas the AILA beamformer employs only 40 sensors, a savings of 8 sensors or 20 percent.

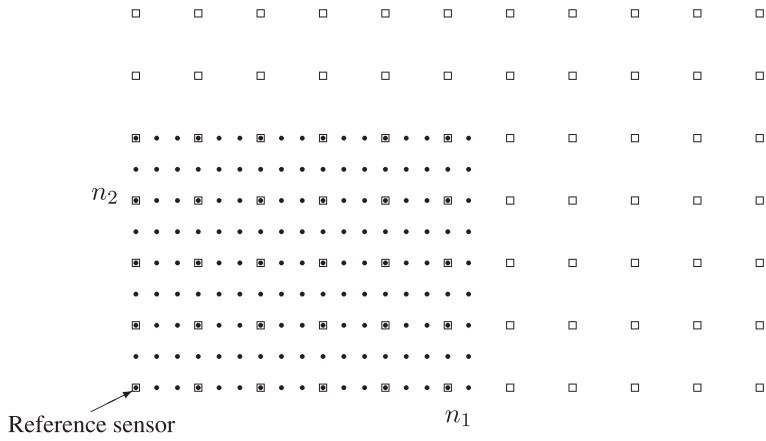

Figure 11. A typical active 2D array comprises one 11×7 sparse transmitting array (solid circles) and one 17×9 dense receiving array (blank squares) with $M_1 = 3$ and $M_2 = 2$.

5. Active two-dimensional array beamforming

Two-dimensional (2D) FIR filter design using the FRM technique was explored in [13], [18], in which the 2D frequency plane is divided into a number of complementary regions. By properly designing the masking filters, 2D FIR filters with sharp transitions can be synthesized. In this section, we generalize the beamforming method described in Section 4 to 2D active array beamformers with separable aperture functions.

A layout of an active 2D array is shown in Figure 11 with a reference sensor located at the left bottom corner. The receiving array is an $(N_{m_1} \times N_{m_2})$-sensor array with intersensor spacing $d = \lambda/2$ in both the n_1 and n_2 directions. The transmitting array is an $(N_{a_1} \times N_{a_2})$-sensor array with intersensor spacings $M_1 d = M_1\lambda/2$ and $M_2 d = M_2\lambda/2$ in the n_1 and n_2 directions, respectively.

Assume that an object is located in the direction of (θ_a, θ_e) in the far field, where θ_a and θ_e are the azimuth angle and the elevation angle, respectively. The transmitted narrowband signal with center frequency ω_o, weighted with the transmitting aperture function $\{h_t(n_1, n_2)\}, 0 \le n_1 \le N_{a_1} - 1, 0 \le n_2 \le N_{a_2} - 1$, strikes the object in the far field at different phases, leading to the scattered signal

$$x_s(k) = \sum_{n_1=0}^{N_{a1}-1} \sum_{n_2=0}^{N_{a2}-1} e^{j\omega_o k} h_t(n_1, n_2) e^{-2\pi \mathbf{k}^T \mathbf{r}/\lambda}, \tag{22}$$

where $\mathbf{k}$ is a unit direction vector pointing to the reference sensor of the transmitting array from the object and $\mathbf{r}$ is a sensor location vector with respect to the

reference sensor. Both vectors can be expressed in Cartesian coordinates

$$\mathbf{k} = [k_x \;\; k_y \;\; k_z]^T = [\cos\theta_a \sin\theta_e \;\; \sin\theta_a \sin\theta_e \;\; \cos\theta_e]^T,$$
$$\mathbf{r} = [r_x \;\; r_y \;\; 0]^T = [M_1 n_1 d \;\; M_2 n_2 d \;\; 0]^T,$$

where $[\cdot]^T$ represents the transpose operation. Assume that the transmitting aperture function is separable,

$$h_t(n_1, n_2) = h_{a_1}(n_1) h_{a_2}(n_2). \tag{23}$$

The scattered signal can be simplified as

$$\begin{aligned} x_s(k) &= \sum_{n_1=0}^{N_{a_1}-1} \sum_{n_2=0}^{N_{a_2}-1} e^{j\omega_o k} h_{a_1}(n_1) h_{a_2}(n_2) e^{-\frac{2\pi M_1}{\lambda} k_x n_1 d} e^{-\frac{2\pi M_2}{\lambda} k_y n_2 d} \\ &= e^{j\omega_o k} H_{a_1}(M_1\phi_1) H_{a_2}(M_2\phi_2), \end{aligned} \tag{24}$$

where $\phi_1 = \pi k_x$ and $\phi_2 = \pi k_y$. The scattered signal is then resampled by the receiving array and weighted with the aperture function $\{h_r(n_1, n_2)\}$. Assume that $h_r(n_1, n_2)$ is also separable as $h_r(n_1, n_2) = h_{ma_1}(n_1) h_{ma_2}(n_2)$. The effective response can be expressed as

$$H_{aa}(\phi_1, \phi_2) = H_{a_1}(M_1\phi_1) H_{a_2}(M_2\phi_2) H_{ma_1}(\phi_1) H_{ma_2}(\phi_2). \tag{25}$$

As both transmitting and receiving aperture functions are separable, the whole spectrum ($-1 \le k_x, k_y \le 1$) is divided into four regions. These four regions form a complementary set. Thus, in 2D active array beamforming, four excitations are needed, as shown in Figure 12. In addition to the effective response shown in (25), the other three effective responses are

$$H_{ac}(\phi_1, \phi_2) = H_{a_1}(M_1\phi_1) H_{c_2}(M_2\phi_2) H_{ma_1}(\phi_1) H_{mc_2}(\phi_2), \tag{26a}$$
$$H_{ca}(\phi_1, \phi_2) = H_{c_1}(M_1\phi_1) H_{a_2}(M_2\phi_2) H_{mc_1}(\phi_1) H_{ma_2}(\phi_2), \tag{26b}$$
$$H_{cc}(\phi_1, \phi_2) = H_{c_1}(M_1\phi_1) H_{c_2}(M_2\phi_2) H_{mc_1}(\phi_1) H_{mc_2}(\phi_2). \tag{26c}$$

The effective active array beamformer response, as a summation of (25) and (26), can be written as

$$\begin{aligned} H(\phi_1, \phi_2) &= H_{aa}(\phi_1, \phi_2) + H_{ac}(\phi_1, \phi_2) + H_{ca}(\phi_1, \phi_2) + H_{cc}(\phi_1, \phi_2) \\ &= \big(H_{a_1}(M_1\phi_1) H_{ma_1}(\phi_1) + H_{c_1}(M_1\phi_1) H_{mc_1}(\phi_1)\big) \\ &\quad \times \big(H_{a_2}(M_2\phi_2) H_{ma_2}(\phi_2) + H_{c_2}(M_2\phi_2) H_{mc_2}(\phi_2)\big). \end{aligned} \tag{27}$$

Hence, $H(\phi_1, \phi_2)$ is the product of two 1D active array beamformer responses, which are of the same form as two 1D FRM filters. Similar to our discussion in the previous section, we can then synthesize 2D active beamformers with desirable beampatterns with fewer sensors than using other design techniques, as shown in the following example.

In this example, we simulate the effective beampattern of a 2D array using two 1D FRM filters. In addition to the 1D FRM filter presented in Table 2, another 1D

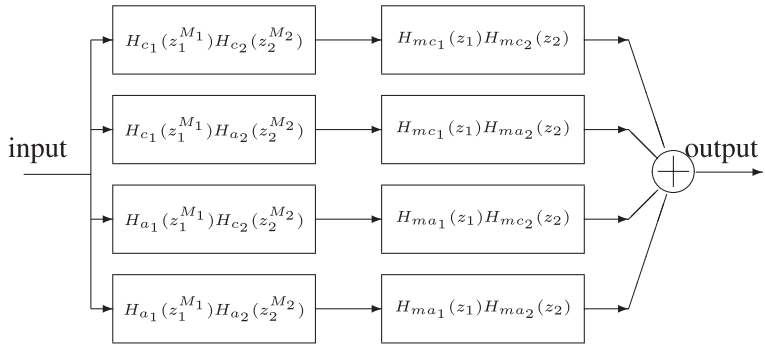

Figure 12. Block diagram of 2D FRM filter synthesis.

Table 4. Frequency specifications of the FRM subfilters with $M = 7$

Subfilter	Filter length	Passband cutoff	Stopband cutoff
$\{h_a(n)\}$	35	0.394π	0.509π
$\{h_{ma}(n)\}$	33	0.342π	0.499π
$\{h_{mc}(n)\}$	33	0.229π	0.358π

FRM filter is designed to meet the same specification as described in Section 4.3; the subfilter specifications are shown in Table 4. 2D aperture functions are formed and applied to the 2D array with a (35×35)-sensor transmitting array and a (39×33)-sensor receiving array. Assume that an object is located in the direction of (θ_a, θ_e) in the far field $(0 \le \theta_a < 2\pi, 0 \le \theta_e \le \pi/2)$. The transmitted signals weighted with the 2D transmitted aperture function strike the object at different phases. The scattered plane wave is resampled by the receiving array and weighted with the corresponding 2D receiving aperture function (see (25) and (26)). For the 2D active array beamforming, four excitations are conducted to complete one cycle. The beamformer output power is recorded at an increment of 1° in both azimuth and elevation angles, and the beampattern is depicted in Figure 13. Finally, to meet the same specification on the beampattern, a 2D beamformer with aperture functions designed using conventional methods, such as the Remez algorithm, would require 215×215 sensors, which is extremely large compared with the number for the proposed active beamforming method.

6. Conclusion

The feasibility of applying the FRM technique in digital array beamforming has been investigated in detail in this paper. Despite the reduced computational complexity in temporal FRM filtering, a large memory to hold the input samples is

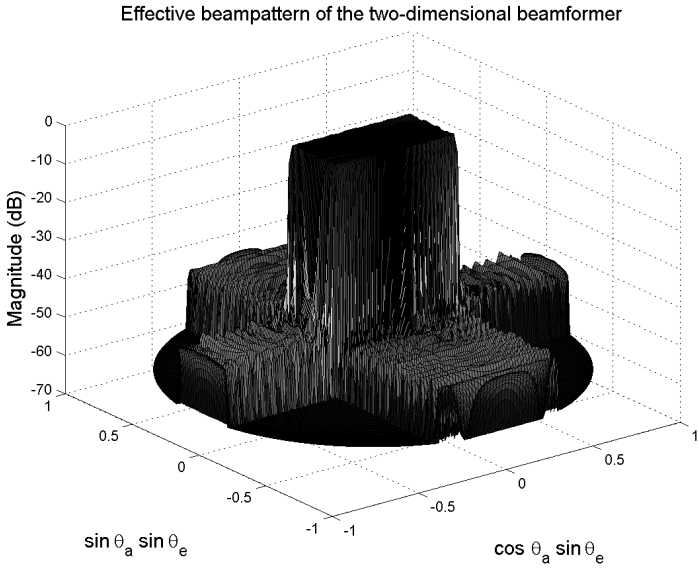

Figure 13. Effective beampattern of the 2D array.

required throughout the filtering process. Because there is no mechanism similar to that of temporal filtering in array beamforming, numerous sensor elements are required to provide enough spatial samples for processing in passive array beamforming. Therefore, it is infeasible to apply the FRM technique in passive array beamforming to reduce the number of sensors while maintaining the same beampattern. However, the FRM technique does find application in active array beamforming by a novel combination with the concept of effective aperture. With fewer sensor elements, a beampattern with sharp transition and low sidelobes can be achieved. The proposed active array beamforming method is also flexible in meeting a specific mainlobe width. The active array beamforming method has also been generalized to 2D active array beamforming and illustrated by simulations.

Acknowledgment

The authors would like to thank an anonymous reviewer for helpful and constructive comments, which helped to improve the presentation of the paper.

References

[1] B. A. J. Angelsen, *Ultrasound Imaging: Waves, Signals and Signal Processing*. Norway: Emantec, 2000.

[2] A. Austeng and S. Holm, Sparse 2-D arrays for 3-D phased arrays imaging—Design methods, *IEEE Trans. Ultrason. Ferroelect. Freq. Contr.*, vol. 49, pp. 1073–1093, Aug. 2002.
[3] S. S. Brunke and G. R. Lockwood, Broad-bandwidth radiation patterns of sparse two-dimensional vernier arrays, *IEEE Trans. Ultrason. Ferroelect. Freq. Contr.*, vol. 44, pp. 1101–1109, Sept. 1997.
[4] G. Franceschetti and R. Lanari, *Synthetic Aperture Radar Processing*, Boca Raton, FL: CRC Press, 1999.
[5] S. M. Gehlbach and R. E. Alvarez, Digital ultrasound imaging techniques using vector sampling and raster line reconstruction, *Ultrason. Imag.*, vol. 3, pp. 83–107, 1981.
[6] S. S. Kidambi and R. P. Ramachandran, Complex coefficient nonrecursive digital filter design using a least-squares method, *IEEE Trans. Signal Process.*, vol. 44, pp. 710–713, Mar. 1996.
[7] M. Z. Komodromos, S. F. Russell, and P. T. P. Tang, Design of FIR filters with complex desired frequency response using a generalized Remez algorithm, *IEEE Trans. Circuits Syst. II*, vol. 42, pp. 274–278, Apr. 1995.
[8] Y. Lian, Complexity reduction for FRM-based FIR filters using the prefilter-equalizer technique, *Circuits Systems Signal Process.*, vol. 22, pp. 137–155, Mar./Apr. 2003.
[9] Y. Lian and C. Z. Yang, Complexity reduction by decoupling the masking filters from the bandedge shaping filter in the FRM technique, *Circuits Systems Signal Process.*, vol. 22, pp. 115–135, Mar./Apr. 2003.
[10] Y. Lian, L. Zhang, and C. C. Ko, An improved frequency response masking approach for designing sharp FIR filters, *Signal Process.*, vol. 81, pp. 2573–2581, Dec. 2001.
[11] Y. C. Lim, Frequency-response masking approach for the synthesis of sharp linear phase digital filters, *IEEE Trans. Circuits Syst.*, vol. CAS-33, pp. 357–364, Apr. 1986.
[12] Y. C. Lim and Y. Lian, The optimum design of one- and two-dimensional FIR filters using the frequency response masking technique, *IEEE Trans. Circuits Syst. II*, vol. 40, pp. 88–95, Feb. 1993.
[13] Y. C. Lim and S. H. Low, Frequency-response masking approach for the synthesis of sharp two-dimensional diamond-shaped filters, *IEEE Trans. Circuits Syst. II*, vol. 45, pp. 1573–1584, Dec. 1998.
[14] Y. C. Lim, Y. J. Yu, H. Q. Zheng, and S. W. Foo, FPGA implementation of digital filters synthesized using the FRM technique, *Circuits Systems Signal Process.*, vol. 22, pp. 211–218, Mar./Apr. 2003.
[15] J. Litva and T. K.-Y. Lo, *Digital Beamforming in Wireless Communications*, Artech House, 1996.
[16] G. R. Lockwood, P.-C. Li, M. O'Donnell, and F. S. Foster, Optimizing the radiation pattern of sparse periodic linear arrays, *IEEE Trans. Ultrason., Ferroelect., Freq. Contr.*, vol. 43, pp. 7–14, Jan. 1996.
[17] G. R. Lockwood, J. R. Talman, and S. S. Brunke, Real-time 3-D ultrasound imaging using sparse synthetic aperture beamforming, *IEEE Trans. Ultrason. Ferroelect. Freq. Contr.*, vol. 45, pp. 980–988, July 1998.
[18] S. H. Low and Y. C. Li, A new approach to synthesize sharp 2-D half-band filters, *IEEE Trans. Circuits Syst. II*, vol. 46, pp. 1104–1110, Aug. 1999.
[19] S.-C. Pei and C.-C. Tseng, A new eigenfilter based on total least squares error criterion, *IEEE Trans. Circuits Syst. I*, vol. 48, pp. 699–709, June 2001.
[20] J. G. Proakis and D. G. Manolakis, *Digital Signal Processing: Principles, Algorithms, and Applications*, Englewood Cliffs, NJ: Prentice-Hall, 1996.
[21] H. L. Van Trees, *Optimum Array Processing*, New York: John Wiley & Sons, 2002.
[22] B. D. Van Veen and K. M. Buckley, Beamforming: A versatile approach to spatial filtering, *IEEE ASSP Mag.*, vol. 5, pp. 4–24, Apr. 1988.
[23] O. T. von Ramm, S. W. Smith, and F. L. Thurstone, Grey scale imaging with complex TGC and transducer arrays, *Proc. Soc. Photo-Opt. Inst. Eng., Med. IV*, vol. 70, pp. 266–270, 1975.